

# CrystEngComm

Accepted Manuscript



This is an *Accepted Manuscript*, which has been through the Royal Society of Chemistry peer review process and has been accepted for publication.

*Accepted Manuscripts* are published online shortly after acceptance, before technical editing, formatting and proof reading. Using this free service, authors can make their results available to the community, in citable form, before we publish the edited article. We will replace this *Accepted Manuscript* with the edited and formatted *Advance Article* as soon as it is available.

You can find more information about *Accepted Manuscripts* in the [Information for Authors](#).

Please note that technical editing may introduce minor changes to the text and/or graphics, which may alter content. The journal's standard [Terms & Conditions](#) and the [Ethical guidelines](#) still apply. In no event shall the Royal Society of Chemistry be held responsible for any errors or omissions in this *Accepted Manuscript* or any consequences arising from the use of any information it contains.

# Synthesis of Microporous/Mesoporous Core-Shell Materials with Crystalline Zeolitic Shell and Supported Metal Oxide Silica Core

*Nima Masoumifard,<sup>a,b,c</sup> Kyoungsoo Kim,<sup>d</sup> Serge Kaliaguine,<sup>b</sup> Pablo M. Arnal,<sup>e</sup> and Freddy Kleitz<sup>\*a,c</sup>*

<sup>a</sup> Department of Chemistry, Université Laval, Quebec City, G1V 0A6, QC, Canada, E-mail: freddy.kleitz@chm.ulaval.ca

<sup>b</sup> Department of Chemical Engineering, Université Laval, Quebec City, G1V 0A6, QC, Canada,

<sup>c</sup> Centre de Recherche sur les Matériaux Avancés (CERMA), Université Laval, Quebec City, G1V 0A6, QC, Canada

<sup>d</sup> Center for Nanomaterials and Chemical Reactions, Institute for Basic Science (IBS), Daejeon 305-701, Korea

<sup>e</sup> Centro de Tecnología de Recursos Minerales y Cerámica (CETMIC) CIC - CONICET La Plata, Centenario y 506, B1897ZCA, M. B. Gonnet, Argentina

## Abstract

An engineered material, possessing a hierarchical porosity in a shape selective manner, was synthesized by placing a microporous silicalite-1 shell over silica microspheres embedding various guest species. Core materials were prepared by dispersing catalytically important metallic species, comprising Co, Mn or Ti, within the mesoporous structure of silica microspheres with different particle and pore sizes. The connectivity of the micro- and mesopore networks and shell integrity of the final core@shell products were studied as the main quality control criteria by varying synthesis parameters, such as core pre-treatments

which include surface modification, seeding and calcination steps and the number of secondary hydrothermal treatments. Depending on the core size and the presence of the guest species, the effectiveness of core seeding is found to be influenced by the chosen surface modification technique, i.e., mesoporous silica microspheres which contain guest species need an additional treatment of chemical functionalization of the external surface with species such as (3-aminopropyl)triethoxysilane, rather than using a simple surface modification with ionic polymers. It is believed that using such chemical treatment can strengthen the adhesion of the seeds to the core surface by providing some additional silanol groups and facilitating hydrogen bonding interactions. It is also shown that depending on the core size, two to four short hydrothermal treatments are required to turn the coated seed crystals into a uniform intergrown shell of silicalite-1 around mesoporous silica microspheres and to avoid aggregation and core dissolution. Such materials with a molecular sieve crystalline shell can be used in a wide variety of applications, particularly for shape-selective adsorption and catalysis purposes.

**Keywords:**

Core@shell, Crystalline shell, Zeolite, Mesoporous silica, Hierarchical porosity, Metal oxide, Shape-selectivity

## Introduction

Core@shell materials are quickly becoming popular in a wide variety of applications especially in the fields of adsorption and catalysis<sup>1, 2</sup>. In addition to profiting from the efficient combination of the inherent properties of each building blocks, a synergetic interaction between the core and the shell compartments could provide new desirable features to the composite entity. In this regard, a core@shell material with a crystalline zeolitic shell can benefit from all extraordinary properties of the zeolite, including high thermal/hydrothermal stability, highly ordered pore structure, large specific surface area and micropore volume, and intrinsic chemical activity. Owing to their excellent resistance under corrosive conditions and molecular sieving property, a zeolitic shell also provides an effective protective layer under harsh operating conditions of some reactions and processes as well as a selective barrier against impurities, poisons, and undesirable reactions. These attributes are particularly attractive to generate more durable composite catalysts with excellent activity and selectivity<sup>3-7</sup>. By implementing a zeolitic coating around microfibers and other macroscopic supports, a robust zeolitic-based *microstructure* can also be manufactured upon techniques similar to those used for core@zeolite preparations. These macroscopic zeolitic assemblies (e.g., *microstructured* catalysts) can practically alleviate problems of using classical zeolitic catalysts, e.g., powdery crystals, microgranules or extruded pellets, in catalytic reactors by improving heat and mass transfer, low pressure drop, corrected flow pattern and avoiding the disadvantages of using inorganic binders<sup>8-10</sup>. Inheriting all these intrinsic properties of a zeolite by the final core@zeolite composite, as well as the emergence of new synergetic features, can be crucial for the core components, especially the ones which are widely used as industrial adsorbents/catalyst supports but suffer from selectivity and stability issues. In particular, high surface area, high pore volume mesoporous silica spheres with the ability of hosting various functional groups (e.g., metals, metal oxides, etc.) when finely covered with a zeolitic shell may hold considerable promise in a variety of applications<sup>11-20</sup>.

Outstanding properties of a zeolitic core@shell are tightly related to the complete shell coverage as well as proper communication between micro/mesopore networks of the constituents. The importance of shell integrity on selective adsorption of small molecules from a hydrocarbon mixture containing butane, toluene, and 1,3,5-trimethylbenzene was demonstrated in the pioneering work of Bouzid et al.<sup>21</sup>, by using a  $\beta$ -

zeolite@silicalite-1 material with maximum shell coverage, i.e., a triple-shell composite. Therefore, the main objective of this study is to implement available techniques toward synthesizing an optimized zeolitic core@shell microsphere, using a mesoporous silica core, hosting various functional groups within its large pores. The desirable final products, non-aggregated core@shell microspheres, should meet a set of quality criteria including the preserved core mesoporosity during the shell formation process, complete shell coverage, pore network connectivity between constituents of the composite, and the absence of free zeolite crystals in the bulk. Although there are few examples of core@zeolite that can be produced by using a one-pot hydrothermal crystallization process<sup>22-26</sup>, the synthesis of a great number of zeolitic core@shell materials is only viable through a multi-step synthesis route<sup>3, 4, 9, 11, 12, 15, 21, 27-33</sup>. The multistep synthesis route usually involves preliminary adsorption of zeolite nanocrystals onto large core particles followed by growing these nanocrystals in an appropriate synthesis gel mixture<sup>34, 35</sup> (Scheme 1). As the primary element of the final product, the properties of the core constituents, such as core particle size and the presence of the desirable guest species can directly impact the performance of this synthesis route and consequently the quality of the final product. In this sense, the effectiveness of the multistep technique for the synthesis of core@shell materials with mesoporous silica core in either pure form or loaded with guest species is evaluated.

Scheme 1

## Experimental

### Pure Mesoporous Silica@Silicalite-1 Preparation

Using tetraethyl orthosilicate (TEOS) (reagent grade, 98%-Sigma-Aldrich) and tetrapropylammonium hydroxide (TPAOH) solution (1M in H<sub>2</sub>O-Sigma-Aldrich), silicalite-1 nanocrystals with an average size of 70 nm were first synthesized from a gel with molar composition of 9TPAOH: 25TEOS: 480H<sub>2</sub>O: 100C<sub>2</sub>H<sub>5</sub>OH

which was kept at 80 °C for 72 h<sup>36</sup>. Thoroughly washed nanocrystals were finally re-dispersed in distilled water to produce 1 wt% suspension. The pH of the suspensions was adjusted to 9–10 with ammonia solution<sup>28</sup>. Various types of mesoporous silica spheres with different particle and pore sizes (commercial silica gel spheres; SG20: 20-45 μm and SG3: 3 μm and Hexagonal Mesoporous Silica (HMS) spheres: ~1.5 μm) were used as core material. SG20 particles with two different average pore sizes (SG20(I): 7nm and SG20(II); 10 nm) were used. All commercial silica gel spheres were purchased from SiliCycle® Inc. Mono-dispersed HMS spheres were synthesized according to the literature<sup>11, 37, 38</sup>. The as-synthesized HMS particles were calcined at 550 °C for 6 h to remove the organic template from the pores.

After these preliminary steps, pure silica core@shell particles were synthesized by adopting the seeded growth method<sup>11, 21, 27</sup>. Around 0.2 g of mesoporous silica spheres were dispersed in 5 ml distilled water, followed by reversing their negative surface charge upon treating with a 5 ml of 0.5 wt% aqueous solution of cationic low molecular weight poly(diallyldimethylammonium chloride) (PDADMAC) solution (20 wt% in H<sub>2</sub>O-Sigma-Aldrich) under 20 min of stirring. Four centrifugal washings, 45 ml water each step, were done to remove the free polyelectrolytes. Afterward, 5 ml of negatively charged silicalite-1 nanocrystals suspension were added to be adsorbed on the surface of the cores owing to electrostatic interactions. The excess nanocrystals were washed away by performing several cycles of centrifugation and re-dispersion of coated particles using a dilute NH<sub>3</sub>-H<sub>2</sub>O solution (pH 9.5). This intermediate product was dried in an oven at 80 °C overnight and then calcined in air at 550 °C for 5 h. The clear gel for secondary growth step was prepared according to Bouizi et al.<sup>21</sup> with the molar composition of 3 TPAOH: 25 SiO<sub>2</sub>:1500 H<sub>2</sub>O:100 C<sub>2</sub>H<sub>5</sub>OH. The coated core particles were dispersed in 10 g of clear gel by stirring at room temperature for 15 min, followed by hydrothermal treatment at 200 °C for 45 min in a Parr Teflon-lined autoclave. After washing the product for four times with distilled water, the secondary growth step was repeated several times (at least twice) to reach the desirable shell coverage. After cooling, the product was treated with a dilute NH<sub>3</sub>-H<sub>2</sub>O solution (pH 9.5) using ultrasonic bath for 10 min to remove the loosely attached silicalite-1 crystals, rinsed repeatedly with distilled water and dried at 100 °C overnight. The as-synthesized material was calcined at 550 °C for 6 h in air after reaching this temperature at a rate of 1°C min<sup>-1</sup> to remove the TPA<sup>+</sup> template from the zeolite pores.

### Preparation of Metal-Containing Mesoporous Silica Microspheres

Metal ions (M = Mn and Co) were introduced into the porous network of mesoporous silica spheres (i.e. HMS, SG3 and SG20) using the incipient wetness technique. In brief, 0.3 g of mesoporous silica, previously evacuated overnight at 150 °C, were impregnated with a solution containing the proper amount of metal nitrate, dissolved in anhydrous ethanol, i.e., cobalt nitrate hexahydrate (Co(II)(NO<sub>3</sub>)<sub>2</sub>·6H<sub>2</sub>O, Alfa Aesar) or manganese nitrate tetrahydrate (Mn(II)(NO<sub>3</sub>)<sub>2</sub>·4H<sub>2</sub>O, Alfa Aesar). The concentration of the impregnation solution was adjusted to provide M/Si molar ratio ratios between 0.05 and 0.2. Solution volumes equal to 80 % of the pore volume of the corresponding mesoporous silica sphere, as measured by N<sub>2</sub> physisorption, were used for each impregnation. Then, the materials were dried overnight at 40 °C and calcined at 500 °C with a 1 °C min<sup>-1</sup> ramp for 3 h under air atmosphere.

Titanium- (Ti) containing mesoporous silica spheres were prepared using titanium (IV) butoxide (TNBT, reagent grade, 97%-Sigma) as the titanium precursor and acetylacetonate (acac, 98%-Sigma) as a chelating ligand<sup>39, 40</sup>. Around 0.3 g of mesoporous silica spheres, totally dried prior to use, were dispersed in 8 ml dry toluene under inert atmosphere. The TNBT (60 μl), acac (105 μl) and 1 ml dry ethanol were quickly pre-mixed in a glass vial and then added to silica suspension in a drop-wise manner while stirring. The final mixture was stirred in an oil bath at 80 °C overnight. The solid products were recovered by centrifugation, quickly washed with 50 ml of anhydrous ethanol, and dried in air at 70 °C overnight. Finally, the yellow powder was calcined at 500 °C for 3 h.

The materials loaded with metals are referred to as M,SiO<sub>2</sub> where M is Co, Mn or Ti and SiO<sub>2</sub> is HMS, SG3, SG20(I) or SG20(II).

### Preparation of Supported Metal Oxide Mesoporous Silica@Silicalite-1

An additional grafting of –NH<sub>2</sub> groups on the external surface of the spheres was used in order to modify the external surface of the metal- containing core particles. Typically, 0.1 g of mesoporous silica supported metal oxide, suspended in 10 ml of dry toluene, was placed in a 25 ml round bottom flask equipped with a

condenser. A solution of excess amount of (3-aminopropyl)triethoxysilane (APTES, 99 %-Sigma) in 5 ml of dry toluene was added dropwise to the dispersed particles under continuous stirring. After complete addition of the organosilane precursor, the reaction mixture was kept under refluxing conditions for about 6 h in inert gas atmosphere. After cooling, the solid was washed with toluene (10 ml) and ethanol (20 ml). The final product was dispersed in 5 ml ethanol without drying. Afterward, 5 ml of silicalite-1 nanocrystals suspension, 1 wt% in ethanol, were added and stirred for 1 h at ambient temperature. The free and loosely attached nanocrystals were removed by performing several cycles of centrifugation (2000 rpm, 5 min) and re-dispersion of the coated particles in ethanol until reaching highly clear supernatant. This intermediate product was dried in an oven at 80 °C overnight and then calcined in air at 550 °C for 5 h. Using the calcined product, supported-metal oxide mesoporous silica@silicalite-1 was synthesized following a procedure similar to the one used for pure mesoporous silica microspheres, described above.

For the sake of comparison, surface modification of the metal-containing core particles was also performed using single layer of a cationic polyelectrolyte or multilayers of cationic/anionic polyelectrolytes. The former method, using positively charged PDADMAC solution was performed according to a previously reported protocol<sup>11, 21, 27</sup> and described briefly above for pure silica core@shell preparation. As a second alternative method, positively charged PDADMAC and anionic poly (styrenesulfonate, sodium salt) (PSS) (Sigma) solutions (0.5 wt% in water) were alternately used to form PDADMAC/PSS/PDADMAC polyelectrolyte layers on the core particles. After each step, the particles were thoroughly washed with water (four centrifugal washings, 45 ml water each step) to remove the free polyelectrolytes. The surface modified particles obtained by either of the two methods, were coated with seeds and used to produce core@shell material following a technique similar to described above for pure silica core@shell preparation.

### Materials Characterization

Powder X-ray diffraction patterns of all samples were recorded using a Siemens powder diffractometer (40 kV, 40mA) with CuK $\alpha$  radiation ( $\lambda = 1.54059 \text{ \AA}$ ). Scanning electron microscopy (SEM) studies were performed using a JEOL JSM-840A scanning electron microscope. High resolution scanning electron

microscopy images (HR-SEM) were taken with a Verios 460 (FEI) at a landing voltage of 1 kV in deceleration mode (stage bias voltage: 4 kV) (KAIST, Daejeon, Republic of Korea). Elemental mapping of the cross-section of samples was performed using energy-dispersive X-ray spectroscopy (EDS) attached to the HR-SEM instrument at 5 kV. The samples were mounted onto an SEM specimen holder using a carbon tape without metal coating. For cross-sectional imaging, the samples were smashed using an agate mortar and pestle before mounting on the holder. Nitrogen adsorption-desorption isotherms were measured at liquid nitrogen temperature (-196 °C), using a Quantachrome Autosorb-1 adsorption analyzer. Prior to the measurements, the non-calcined and calcined samples were evacuated at 80 °C and 200 °C, respectively, for at least 12 h, under the vacuum, provided by a turbomolecular pump. The linear part of Brunauer-Emmett-Teller (BET) plot was used to calculate the specific surface area. Total pore volume of micropores and mesopores was estimated from the amount of nitrogen adsorbed at  $P/P_0 = 0.95$ . For advanced porosity analysis, cumulative pore volumes and pore size distributions were determined by using non-local density functional theory (NLDFT) method applying the NLDFT metastable adsorption branch kernel and considering sorption of nitrogen at -196 °C in silica as a model adsorbent and cylindrical pores as a pore model. Micropore volumes of the zeolites and core@shell materials, as well as their pore size distributions, were determined using NLDFT method. The Quantachrome Autosorb-1 1.55 software was used for data interpretation. X-ray photoelectron spectroscopy (XPS) spectra were collected on a KRATOS Axis-Ultra electron spectrometer (UK) using a monochromatic Al K $\alpha$  X-ray source at a power of 300 W. Powder was placed in a clean copper sample holder (cup). No treatment was performed on the sample other than normal vacuum pumpdown. Electrostatic charge was neutralized with the integrated very low energy electron flood gun, the parameters of which were set to optimize energy resolution and counting rate. Survey scans were recorded with a pass energy of 160 eV and a step size of 1eV. The data were used for elemental analysis and the calculation of apparent concentration. Calculation of the apparent relative atomic concentrations was performed with the CasaXPS software.

## Results and Discussion

The present contribution aims at monitoring how the parameters of the common multistep synthesis technique of the core@shell materials affect the major characteristics of the final product. The effect of surface modification techniques and number of secondary growth steps, as the two major stages of synthesizing core@zeolite through a multistep fashion, on the quality of the resulting core@shell material are investigated, using different sizes of mesoporous silica microspheres, with or without metallic guest species.

### Effect of Secondary Growth Repetitions Using Pure Silica Cores

The efficacy of surface modification by coating the core materials using ionic soluble polymers has been demonstrated in several research studies<sup>28, 41</sup>. Our previous study showed that this technique is highly efficient in providing required interactions between the nanozeolites and pure mesoporous silica spheres as used in this study<sup>11</sup>. Therefore, in the current section, the impact of the number of consecutive secondary growth steps, e.g., 2-4 times, on the quality of the final product is discussed. Different core particles with different sizes and textural properties, i.e., commercial silica gel spheres and hexagonal mesoporous silica microspheres (HMS), were used as core materials. Figures S1a-c and S2a-d (Electronic Supplementary Information) show the scanning electron microscopy (SEM) images and nitrogen physisorption isotherms (-196 °C), respectively, obtained for all the mesoporous silica cores used in the present study. Their textural properties are reported in Table 1. The synthesized HMS particles showed uniform size and shape with mean diameter around 1.5  $\mu\text{m}$  (Figure S1a). Commercial silica gel spheres SG3 and SG20 (Silicycle Inc, Canada) showed wider particle size distributions than HMS, especially SG20 with a size range of 20 to 45  $\mu\text{m}$  (Figures S1b and S1c). All the mesoporous silica cores showed a type IV nitrogen adsorption/desorption isotherm, characteristic of mesoporous solids, with a significant uptake in the relative pressure region of 0.6–0.8 for silica gel and 0.2–0.3 for the HMS particles, attributed to capillary condensation effect. The maximum point in the corresponding mono-modal pore size distribution curve, obtained from NLDFT analysis, was centered at the pore sizes of 3, 6, 6 and 8 nm for HMS, SG3, SG20(I) and SG20(II) with

smaller and larger pores, respectively (Table 1). More details about their porous structure including pore size distribution curves can be found in our previous report<sup>11</sup>.

Scanning electron microscopy images of the seeded HMS and SG particles, depicted in Figure S3a-c, show that the seeding process in slightly basic condition did not irreversibly change the overall morphology of the core particles. Textural properties of the seeded cores were also evaluated by nitrogen physisorption. Figures S3d and S3e compare the results for HMS spheres after and before seeding, as an example. Although the presence of non-calcined silicalite-1 seeds and probably remaining polymeric species from the coating step reduced the pore volume of the seeded cores, the shape of the isotherm and corresponding cumulative pore volume remained similar to those observed for pure HMS. The pore size distribution curve was slightly broadened which may be attributed to the presence of polymers used for the coating and interstitial spaces between nanoparticles. However, the pore network structure of the core remained quite intact, as expected.

The shell, which was initially formed by deposited zeolite nanocrystals around the positively-charged external surfaces of the spheres using single layer of PDADMAC polyelectrolyte, was gradually converted into a polycrystalline intergrown silicalite-1 shell through successive hydrothermal treatments of 45 min each in a gel containing tetraethyl orthosilicate (TEOS)/tetrapropylammonium hydroxide (TPAOH). This repetitive quick conventional hydrothermal treatment is a crucial factor to avoid the core dissolution and aggregation of final products in comparison to longer vapor phase transport (VPT) treatment which was previously used to generate hollow zeolites using mesoporous silica spheres as core<sup>41, 42</sup>. Although hollow zeolites are of great importance in a variety of applications<sup>43, 44</sup>, preserving the mesoporous silica core in a well-connected micro/mesoporous composite network can also provide several advantages including high mesopore volume and high surface area which allows having either evenly-distributed functional groups supported in a highly accessible network for reactants or high chemical/physical adsorption capacity of molecules of interest on the core surface sites. Figure 1 shows SEM images of various mesoporous silica microspheres after two and four consecutive secondary growth steps. According to literature, two successive hydrothermal treatments in silica-containing gel are necessary for achieving an acceptable level of shell coverage over  $\beta$ -zeolite cores<sup>21, 27</sup>. We observed that the same rule holds true when mesoporous

silica spheres are used, especially for the smaller ones, i.e., HMS and SG3 (Figures 1a,1c and 1e). Increasing the number of secondary growth steps for the smallest cores, i.e., the HMS spheres, not only did not provide any improvements in shell coverage, but also led to the formation of highly aggregated particles and hollow spherical caps. The formation of these additional particle species is attributed to a complete dissolution of mesoporous silica from the interior region in bare spots on external surface where the initial coating of seed was not dense enough (Figure 1b). In contrast to small HMS core particles, SEM imaging inspection of the core@shell samples with larger SG cores did not show any aggregation or hollow bodies after repeating the hydrothermal treatments for four times (Figures 1c-1f).

Nitrogen physisorption isotherms were measured for the core@shell products prior to the final calcination steps and used to assess the shell coverage quality and uniformity. Figures 2 and S4 compare the isotherms, obtained by N<sub>2</sub> sorption measurements after different numbers of hydrothermal treatment steps. Since all the micropores on the shell sides are totally filled and blocked with structure-directing agent (SDA) molecules, the internal porosity of non-calcined core@shell products would not be accessible, proving a perfect zeolitic shell coverage. Assuming that the mass ratio between silicalite-1 and the core for samples with different core sizes remains comparable after each secondary growth step, this property, low gas uptake by non-calcined samples, can be used to determine the number of secondary growth required for each particle. From the lowest N<sub>2</sub> uptake obtained for each sample (Figures 2 and S4), it is clear that the smaller the particle is, the less hydrothermal treatments is required to achieve reasonable shell completeness, which could thus efficiently prevent N<sub>2</sub> to access the internal mesoporosity of the non-calcined core@shell products. For HMS particles, this is achieved after two times of hydrothermal treatments, while SG20 evidently needs four hydrothermal treatment sequences. SG3 particles also reach acceptable level of shell coverage after the second hydrothermal treatment.

Nitrogen physisorption data for calcined core@shell products can be used to evaluate the pore network connectivity between the constituents. Textural properties of the final calcined core@shell materials were also evaluated for all the different core materials used and presented in Table 1. After calcination, the SDAs will be burned out and both core mesoporosity and shell microporosity are becoming accessible. In comparison to the pristine cores (Figure S2), the isotherm of the calcined core@shell material (Figures 2

and S4) showed a noticeable reduction in nitrogen uptake at higher values of  $P/P_0$  (capillary condensation region), relative to that of the mesoporous silica spheres, showing that relative mesopore contribution in the final porosity was drastically decreased by the dense microporous silicalite-1 shell. However, capillary condensation can still be observed at high relative pressures ( $P/P_0 > 0.6$ ) indicating the presence of mesopores, and it is accompanied by a complex hysteresis behavior, which we tentatively attribute to cavitation effect<sup>45, 46</sup>. It is also observed that the ratio between mesoporosity and microporosity is a function of core size, larger particles showing higher ratio than smaller ones (Table 1). In other words, by using larger core particles, the contribution of micropores to the total porosity of the core@shell products decreases. This is evident by comparing the micropore volume and surface area of submicron silicalite-1 aggregates, listed in Table 1, with the values reported for calcined core@shell products with different core sizes. Moreover, large mesopores (pore sizes ~16 nm), formed upon aggregation of small crystals during drying and calcination of the silicalite-1 sample and contributing to large total pore volume and surface area, have completely vanished in the core@shell products, confirming a tight intergrowth of nanocrystals leading to the formation of a zeolitic shell free of interstitial pores.

Figure 2

In conclusion, using pure mesoporous silica microspheres, the shell coverage and uniformity is found to be a function of core particle size, i.e., larger particles such as SG20 benefit from a nice and uniform shell of silicalite-1 if the secondary growth step is repeated for at least four times.

### **Effect of Surface Modifications Using Metal-Containing Cores**

The results obtained for the pure silica core@shell materials can be used for synthesizing core@shell materials with guest species, e.g., metal oxides, nanoparticles, since the presence of guest species is not

expected to affect the number of secondary growth steps required for deposited nanocrystals to grow. To illustrate this feature, various metals were introduced into the pore structure of mesoporous silica spheres using impregnation techniques. Figures S1d-f and S2e-g (ESI) show the SEM images and nitrogen physisorption isotherms, respectively, obtained for some of guest-containing mesoporous silica cores used in this study. Following exactly the same procedure as described above for synthesizing pure silica @silicalite-1 samples, the metal-containing (e.g., Co, Mn) particles were then used as core for synthesizing metal-containing core@shell microspheres. SEM images of the final products are shown in Figure S5. Unexpectedly, in contrast to pure silica @silicalite-1 samples, most of the synthesis attempts failed to provide a perfect coverage, especially for the larger particles (e.g., SG). This was probably caused by inefficient seeding of the external surface of the cores due to lack of proper interaction between the core particles and silicalite-1 nanocrystals. In other words, introducing metal oxide might change the surface properties of particles. Surface modification is indeed crucial for preparing high quality core@shell materials by establishing the required levels of attractive interactions between the zeolite nanocrystals and the external surface of the core, leading to high density and firm adhesion of the seeds on the surface. The low density of nanocrystals on the surface seems to spoil the possibility of forming a well-intergrown uniform shell upon hydrothermal treatment. In addition, it cannot allow the shell to play the protective role of coated seeds toward hindering the dissolution of the core or leaching of possible guest species during the course of secondary hydrothermal treatments<sup>21</sup>. Loose interactions between the seeds and the core surface would result in an incomplete coverage of zeolitic shell and the formation of discrete bulk crystals that would arise from detached seeds which later grow freely inside the medium used for the secondary hydrothermal step. Complete removal of these bulk crystals, especially when their sizes are comparable to that of the core@shell product imposes some difficulties in purification of the final core@shell product. In addition, the growth of this bulk crystals freely consumes reaction nutrients required for the formation and uniform growth of the zeolitic shell.

One strategy to improve the formation of an homogenous shell is the layer-by-layer adsorption of ionic polymers of opposite charges before seeding with nanozeolites<sup>47-51</sup>. Increasing the thickness of polymeric coating around the core particles can possibly enhance the interaction between negatively charged nanocrystals and positive core surfaces. Therefore, three layers of polymer in the order of

PDADMAC/PSS/PDADMAC were placed around the cores. Figure S6 shows that this method slightly improved the coverage, however, it led to large number of nanocrystals formed in the bulk and irregular surface of the final product. Moreover, due to the time consuming multistep procedure, it is often rather tedious to use this technique<sup>52</sup>.

Alternatively, we explored the functionalization of the external surface of the particles using APTES which provides adequate solution to this problem by increasing the zeta potential of the silica particles from highly negative toward positive values<sup>53</sup>, improving the electrostatic interactions of nanocrystals and silica particles during the seeding step. In addition, this modification can provide amine functional groups along with some free silanol groups on the external surface which can help anchoring the seeds to the surface via hydrogen bonding and/or upon condensation during a short calcination before secondary growth. Core surface modification via functionalization of the external surface with amine moieties has previously been used for synthesizing core@shell catalysts using millimetre-size cores<sup>13, 14, 16, 54</sup>. Using this method, it was observed that the detachment of the seeds from external surface was avoided leaving no bulk crystals in as-synthesized sample after secondary growth steps. However, reaching large concentration of functional groups might not be possible due to high porosity of the mesoporous cores and diffusion of the organic moieties into the pore system. Figure S7 shows the results obtained when only APTES grafting was used to modify the surface of core particles which reveals a partial coverage of silica surface even after 3-4 secondary hydrothermal steps.

Finally, a single-step surface modification with polyelectrolytes was also attempted to ensure the perfect coverage by increasing the density of nanocrystals on the core external surface. This time, Figures 3 and S8 show clear improvement in the zeolitic shell coverage after adding APTES grafting and seeding steps to the method previously used for coating pure silica spheres (Scheme 1). The corresponding SEM images confirmed the absence of abundant silicalite-1 crystals in the bulk while all particles are entirely coated with well-intergrown shell of silicalite-1 (Figure 3 and S8).

Figure 3

Moreover, the preservation of the structure of the mesoporous silica supports was studied by breaking the particle through simple mechanical grinding. The resulting SEM images (Figures 4a-d and S9) reveal that the metal-containing core structures survived during multiple hydrothermal treatments, owing to the protective layer of silicalite-1. Figures 4a-d and S9 clearly show the interface between the microporous crystalline shell and the mesoporous silica core. Moreover, from these images of broken particles, the shell thickness of the final product could be estimated to be smaller than about 0.5-1  $\mu\text{m}$ , varying with the size of the selected core particles, i.e. larger particles allow the growth of a thicker shell. Regarding the required number of secondary growth steps, similar results were obtained as described above for pure silica core@shell materials. Nevertheless, Figures 4e and 4f show that increasing the number of secondary growth steps can finally lead to a slight aggregation of the particles, cracking of the shell and some dissolution of the core material.

Figure 4

Again, nitrogen sorption measurements can be used to show that the zeolitic layer efficiently restricts the access of nitrogen molecules to the inner channels of the mesoporous silica cores. To analyze the entirety of silicalite-1 shell, nitrogen adsorption isotherms were obtained for as-synthesized samples (Figures 5 and S10). The continuity of such a zeolite shell should guaranty a shape selectivity of the final hierarchical material, however, minor deviations from perfect shell coverage by appearance of pinholes and small cracks are not expected to prevent shape selectivity<sup>55</sup>. Non-calcined samples showed very little nitrogen uptake, showing that the pore-blocked zeolitic layer efficiently restricted the access of nitrogen molecules to the inner channels of the mesoporous silica core. However, upon calcination both micropores of the silicalite-1 layer and mesopores of the core are made accessible by the probe molecules. The textural properties of the different calcined core@shell spheres obtained by nitrogen physisorption measurements

are summarized in Table 1. It should also be noted that the SG20 particles with larger average pore size (SG20(II)) have not been used for synthesis of metal-containing core@shell catalysts owing to their lower surface area and some mechanical stability issues.

Figure 5

The cumulative pore volumes and pore size distributions of the pristine silica gel (SG3 and SG20(I)) and their corresponding supported-metal oxide and core@shell products were obtained by using the nonlocal density functional theory (NLDFT) method ( $N_2$  sorption in cylindrical silica pores, adsorption branch) and are depicted in Figure 6. The mesoporous silica gel spheres presented the largest pore volume and a narrow pore size distribution with a maximum centered between 6 and 7 nm. Upon introducing metallic species into the pore networks of silica gel particles, the total pore volume slightly decreased, without considerable change in the pore size distribution. In contrast, the pore size distribution of the final core@shell material showed the emergence of small pores in microporous region (pores smaller than 2 nm) which is associated to the silicalite-1 shell. Mesopores (pores larger than 2 nm) are also apparent in the pore size distribution curves which showed wider distribution compared to the parent silica particles, however, the maximum points of the curve are still positioned between 6 to 7 nm, as observed for the silica gel particles. There is another maximum point in the mesopore region which could here be an artifact, arising from the complex pore network connectivity between the mesoporous core and microporous shell.

Figure 6

Survey XPS spectra were used for measuring the elemental composition of the powdery samples surfaces in the case of Co modified materials (Figure 7). A section of the full spectra, corresponding to the expected position for Co(2p) peaks were magnified and plotted in Figure 7, showing two Co2p peaks at approximately 778 eV and 793 eV for bare metal-loaded SG20(I). Although the exact determination of Co oxidation state might not be possible using this survey spectrum and needs a high-resolution analysis, using this technique, the guest species which could possibly leached out during the shell formation steps or attached on the external surface of un-coated particles can be detected. Apparent relative concentrations in atomic % were also estimated based on each survey spectrum and used to calculate the M/Si ratio which are presented with the corresponding spectrum in Figure 7. As can be seen in Figure 7, Co species were detected in bare metal-containing sample and one of the failed syntheses with a partial silicalite-1 coverage. However, the core@shell products with complete zeolitic shell did not present any metal species within the Co detection limit, which was estimated to be of the order of 0.05 atomic % (Figure 7).

Figure 7

The radial distribution of guest metal species was analysed by EDS elemental mapping for two Co-containing core@shell samples at two different initial compositions (exactly same samples which were used for XRD and XPS surface analyses). Particles were broken by simple grinding using a mortar and pestle. Figures 8b and 8d show that Co concentration on the core region stays constant and uniform and then drop to low quantities, close to zero, at the interface between silicalite-1 shell and mesoporous silica core. Grinding, as an intrusive method, could contaminate the silicalite-1 shell by pushing metal oxide traces into the shell side. It should also be noted that the sharp fluctuation at the core and shell interface, shown in Figure 8h, can be attributed to the gap between these two parts<sup>30</sup>, probably caused by destructive effect of grinding process on large core@shell material with SG20 microsphere as core. The atomic metal to silicon ratio were also measured using EDS analysis as 4 and 1 % for Co,SG3@silicalite-1 and Co,SG20(I)@silicalite-1, respectively, while XPS survey did not show any Co species on the external

surface of the shell and in the bulk. The structural characteristics of these Co-containing core@shell were also studied using XRD (Figure S11). Most of the peaks observed in XRD patterns, i.e., peaks at  $2\theta=7.5-9.5$ ,  $23-24$  and  $30$  degree, correspond to the crystalline structure of silicalite-1 shell, as compared to simulated MFI diffractograms. Considering the low concentration of the guest species in Co,SG20(I)@silicalite-1, cobalt oxide did not appear in the powder XRD pattern, while in the case of Co,SG3@silicalite-1 with higher concentration a broad peak appeared on the diffractograms. The maximum point is centred at  $36.9$  degree which is characteristic of  $\text{Co}_3\text{O}_4$ , corresponding to 311 reflection.

Figure 8

## Conclusion

Formation of well-defined  $\text{SiO}_2$ @zeolite particles requires the ability to grow a polycrystalline, zeolitic shell around each mesoporous silica cores — destruction of the spherical template and intergrowth among different particles ought to be avoided. Our work showed that  $\text{SiO}_2$ @silicalite-1 can be formed when coating mesoporous spheres with PDADMAC, adsorbing silicalite-1 nanocrystals, and then hydrothermally treating smaller microspheres (i.e., HMS and SG3) at least two times — more treatments leads to particle aggregation and core dissolution for HMS particles — and largest spheres (SG20) four times. Therefore, regarding these pure silica cores, the required number of secondary growth steps is directly correlated to the size of the core particles, i.e., two successive short hydrothermal treatments provide a uniform shell coverage for small microspheres like HMS particles, while larger ones may require more steps. Furthermore, when supporting metal oxides inside the mesopores of the spheres before the formation of the zeolitic shell, the creation of well-defined M, $\text{SiO}_2$ @silicalite-1 core@shell spheres required an additional external surface functionalization of the spheres with APTES. Accordingly, these results can be used to obtain efficient adsorbents, catalysts and zeolitic microstructures exhibiting hierarchical architecture with various functional groups, evenly embedded within mesoporous core compartment and protected by a shape selective microporous zeolitic shell.

## Acknowledgements

The authors acknowledge financial support from the National Science and Engineering Research Council (Canada) and the Fonds québécois de la recherche sur la nature et les technologies (FRQNT).

## Electronic Supplementary Information (ESI) available

Additional characterization data of the different samples: SEM images, N<sub>2</sub> adsorption-desorption isotherms and powder XRD patterns. See DOI:

## References

1. R. Ghosh Chaudhuri and S. Paria, *Chem. Rev.*, 2011, **112**, 2373 – 2433.
2. H. Wang, L. Chen, Y. Feng and H. Chen, *Acc. Chem. Res.*, 2013, **46**, 1636-1646.
3. J. Zhang, T. Zhang, X. Zhang, W. Liu, H. Liu, J. Qiu and K. L. Yeung, *Catal. Today*, 2014, **236**, 34-40.
4. A. Ghorbanpour, A. Gumidyala, L. C. Grabow, S. P. Crossley and J. D. Rimer, *ACS Nano*, 2015, **7**, 4006–4016.
5. T. Du, H. Qu, Q. Liu, Q. Zhong and W. Ma, *Chem. Eng. J.*, 2014, **262**, 1199–1207.
6. X. Wang, Y. Cui, Y. Wang, X. Song and J. Yu, *Inorg. Chem.*, 2013, **52**, 10708–10710.
7. J. Wang, D.-M. Do, G.-K. Chuah and S. Jaenicke, *ChemCatChem*, 2013, **5**, 247-254.
8. J. Ding, L. Han, M. Wen, G. Zhao, Y. Liu and Y. Lu, *Catal. Commun.*, 2015, **72**, 156-160.
9. M. Wen, J. Ding, C. Wang, Y. Li, G. Zhao, Y. Liu and Y. Lu, *Microporous Mesoporous Mater.*, 2016, **221**, 187-196.
10. X. Wang, M. Wen, C. Wang, J. Ding, Y. Sun, Y. Liu and Y. Lu, *Chem. Commun.*, 2014, **50**, 6343-6345.
11. N. Masoumifard, P. M. Arnal, S. Kaliaguine and F. Kleitz, *ChemSusChem*, 2015, **8**, 2093-2105.

12. E. A. Khan, A. Rajendran and Z. Lai, *Chem. Eng. Res. Bull.*, 2013, **16**, 1-15.
13. X. Wang, X. Zhang, Y. Wang, H. Liu, J. Wang, J. Qiu, H. L. Ho, W. Han and K. L. Yeung, *Chem. Eng. J.*, 2011, **175**, 408-416.
14. N. Jiang, G. Yang, X. Zhang, L. Wang, C. Shi and N. Tsubaki, *Catal. Commun.*, 2011, **12**, 951–954.
15. E. A. Khan, A. Rajendran and Z. Lai, *Ind. Eng. Chem. Res.*, 2010, **49**, 12423-12428.
16. J. Zhou, X. Zhang, J. Zhang, H. Liu, L. Zhou and K. Yeung, *Catal. Commun.*, 2009, **10**, 1804-1807.
17. G. Yang, Y. Tan, Y. Han, J. Qiu and N. Tsubaki, *Catal. Commun.*, 2008, **9**, 2520-2524.
18. G. Yang, J. He, Y. Zhang, Y. Yoneyama, Y. Tan, Y. Han, T. Vitidsant and N. Tsubaki, *Energy Fuels*, 2008, **22**, 1463-1468.
19. G. Yang, J. He, Y. Yoneyama, Y. Tan, Y. Han and N. Tsubaki, *Appl. Catal., A*, 2007, **329**, 99-105.
20. J. He, Y. Yoneyama, B. Xu, N. Nishiyama and N. Tsubaki, *Langmuir*, 2005, **21**, 1699-1702.
21. Y. Bouizi, I. Diaz, L. Rouleau and V. Valtchev, *Adv. Funct. Mater.*, 2005, **15**, 1955-1960.
22. A. L. Yonkeu, V. Buschmann, G. Miehe, H. Fuess, A. M. Goossens and J. A. Martens, *Cryst. Eng.*, 2001, **4**, 253-267.
23. M. Miyamoto, T. Kamei, N. Nishiyama, Y. Egashira and K. Ueyama, *Advanced Materials*, 2005, **17**, 1985-1988.
24. D. He and D. Liu, *RSC Adv.*, 2015, **5**, 5438-5441.
25. M. Okamoto, L. Huang, M. Yamano, S. Sawayama and Y. Nishimura, *Appl. Catal., A*, 2013, **455**, 122–128.
26. Z. Jin, S. Liu, L. Qin, Z. Liu, Y. Wang, Z. Xie and X. Wang, *Appl. Catal., A*, 2013, **453**, 295-301.
27. G. D. Pirngruber, C. Laroche, M. Maricar-Pichon, L. Rouleau, Y. Bouizi and V. Valtchev, *Microporous Mesoporous Mater.*, 2013, **169**, 212–217.
28. V. Valtchev and S. Mintova, *Microporous Mesoporous Mater.*, 2001, **43**, 41-49.
29. V. Valtchev, *Chem. Mater.*, 2002, **14**, 956-958.
30. Y. Bouizi, L. Rouleau and V. P. Valtchev, *Microporous Mesoporous Mater.*, 2006, **91**, 70-77.
31. Y. Bouizi, L. Rouleau and V. P. Valtchev, *Chem. Mater.*, 2006, **18**, 4959-4966.
32. Y. Bouizi, G. Majano, S. Mintova and V. Valtchev, *J. Phys. Chem. C*, 2007, **111**, 4535-4542.
33. E. A. Khan, E. Hu and Z. Lai, *Microporous Mesoporous Mater.*, 2009, **118**, 210-217.

34. V. Valtchev, J. Hedlund, B. J. Schoeman, J. Sterte and S. Mintova, *Microporous Mater.*, 1997, **8**, 93-101.
35. V. Valtchev, *Chem. Mater.*, 2002, **14**, 4371-4377.
36. B. J. Schoeman, K. Higberg and J. Sterte, *Nanostruct. Mater.*, 1999, **12**, 49-54.
37. M. Grün, G. Büchel, D. Kumar, K. Schumacher, B. Bidlingmaier and K. K. Unger, in *Stud. Surf. Sci. Catal.*, eds. G. K. K.K. Unger and J. P. Baselt, Elsevier, 2000, vol. Volume 128, pp. 155-165.
38. A. Dong, N. Ren, W. Yang, Y. Wang, Y. Zhang, D. Wang, J. Hu, Z. Gao and Y. Tang, *Adv. Funct. Mater.*, 2003, **13**, 943-948.
39. F. Bérubé, B. Nohair, F. Kleitz and S. Kaliaguine, *Chem. Mater.*, 2010, **22**, 1988-2000.
40. F. Bérubé, A. Khadraoui, J. Florek, S. Kaliaguine and F. Kleitz, *J. Colloid Interface Sci.*, 2015, **449**, 102-114.
41. A. Dong, Y. Wang, D. Wang, W. Yang, Y. Zhang, N. Ren, Z. Gao and Y. Tang, *Microporous Mesoporous Mater.*, 2003, **64**, 69-81.
42. R. Kanthasamy, K. Barquist and S. C. Larsen, *Microporous Mesoporous Mater.*, 2008, **113**, 554-561.
43. B. Zornoza, O. Esekhiile, W. J. Koros, C. Téllez and J. Coronas, *Sep. Purif. Tech.*, 2011, **77**, 137-145.
44. K. Vanherck, A. Aerts, J. Martens and I. Vankelecom, *Chem. Commun.*, 2010, **46**, 2492-2494.
45. M. Thommes, *Chem. Ing. Tech.*, 2010, **82**, 1059-1073.
46. C. J. Rasmussen, A. Vishnyakov, M. Thommes, B. M. Smarsly, F. Kleitz and A. V. Neimark, *Langmuir*, 2010, **26**, 10147-10157.
47. F. Caruso, R. A. Caruso and H. Möhwald, *Science*, 1998, **282**, 1111-1114.
48. K. H. Rhodes, S. A. Davis, F. Caruso, B. Zhang and S. Mann, *Chem. Mater.*, 2000, **12**, 2832-2834.
49. X. D. Wang, W. L. Yang, Y. Tang, Y. J. Wang, S. K. Fu and Z. Gao, *Chem. Commun.*, 2000, 2161-2162.
50. W. Yang, X. Wang, Y. Tang, Y. Wang, C. Ke and S. Fu, *J. Macromol. Sci., Part A: Pure Appl. Chem., Part A: Pure and Applied Chemistry*, 2002, **39**, 509 - 526.
51. A. Dong, Y. Wang, Y. Tang, N. Ren, Y. Zhang and Z. Gao, *Chem. Mater.*, 2002, **14**, 3217-3219.
52. B. Sun, S. A. Mutch, R. M. Lorenz and D. T. Chiu, *Langmuir*, 2005, **21**, 10763-10769.
53. G. E. Musso, E. Bottinelli, L. Celi, G. Magnacca and G. Berlier, *Phys. Chem. Chem. Phys.*, 2015, **17**, 13882-13894.
54. Q. Lin, G. Yang, X. Li, Y. Yoneyama, H. Wan and N. Tsubaki, *ChemCatChem*, 2013, **5**, 3101-3106.

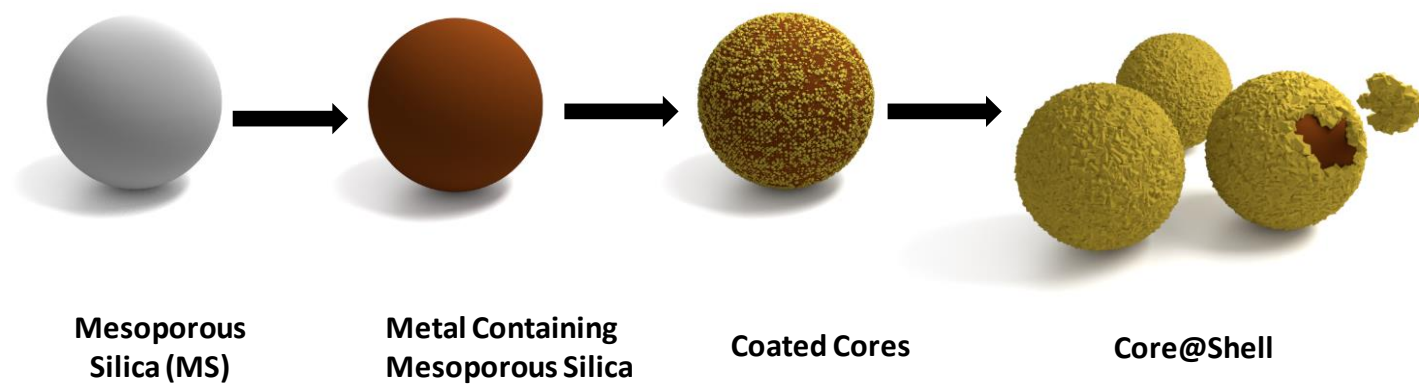
55. N. van der Puil, E. W. Kuipers, H. van Bekkum and J. C. Jansen, in *Stud. Surf. Sci. Catal.*, eds. G. Poncelet, J. Martens, B. Delmon, P. A. Jacobs and P. Grange, Elsevier, 1995, vol. Volume 91, pp. 1163-1171.

Masoumifard, N. *et al.*Table 1- Textural properties of the core@shell materials obtained by performing N<sub>2</sub> physisorption analysis at -196 °C.

Sample	S <sub>BET</sub> <sup>[a]</sup> [m <sup>2</sup> g <sup>-1</sup> ]	Micropore surface area <sup>[b]</sup> [m <sup>2</sup> g <sup>-1</sup> ]	Micropore volume <sup>[c]</sup> [cm <sup>3</sup> g <sup>-1</sup> ]	Pore volume <sup>[d]</sup> [cm <sup>3</sup> g <sup>-1</sup> ]	Maximum mesopore size <sup>[e]</sup> [nm]
HMS (1.5 μm)	780	----	----	0.6	3.3
Silica gel (3 μm)- SG3	453	----	----	0.7	6.2
Silica gel (20-45 μm)- SG20(I)	512	----	----	0.8	6.2
Silica gel (20-45 μm)- SG20(II)	326	----	----	0.8	8 <sup>f</sup>
Silicalite-1 (~ 300 nm)	484	378	0.15	0.55	16
HMS@silicalite-1	430	335	0.13	0.26	3.7, 6
SG3@silicalite-1	280	166	0.08	0.25	3.5, 7.2
SG20(I)@silicalite-1	240	83	0.023	0.27	6.8
SG20(II)@silicalite-1	180	70	0.025	0.24	3.5, 7.4
Ti,HMS@silicalite-1	273	223	0.093	0.14	3.5, 5.6
Co,SG3@silicalite-1	176	115	0.046	0.186	4, 7
Co,SG20(I)@silicalite-1	287	184	0.07	0.27	6.5
Ti,SG20(I)@silicalite-1	300	124	0.043	0.35	6.5

[a] Calculated by using the BET method on relatively low-pressure region. [b] Difference between S<sub>BET</sub> and NLDFT cumulative surface area for pore sizes larger than 2 nm. [c] Calculated using NLDFT cumulative pore volume for pore sizes smaller than 2 nm. [d] Calculated at P/P<sub>0</sub>=0.95. [e] Derived from NLDFT pore size distribution in mesopore region (pore sizes larger than 2 nm). The two values correspond to the two maxima in the pore size distribution curves. [f] Corrected value for the average pore size of SG20 microspheres which were used in our previous study (ref. 11).

Masoumifard, N. *et al.*



**Scheme 1.** Schematic representation of the metal-containing mesoporous silica@silicalite-1 synthesis.

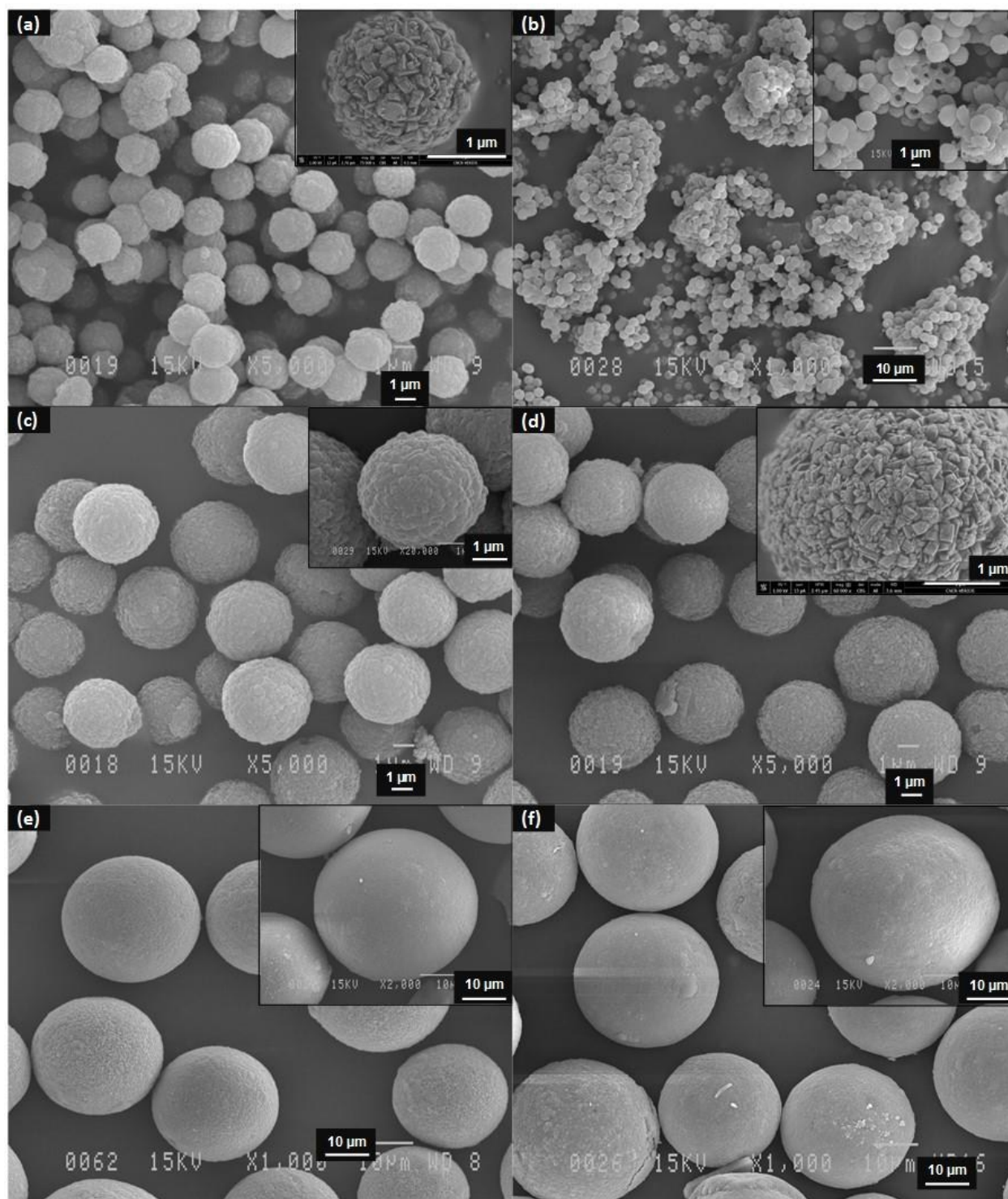


Figure 1- SEM images of (a,b) HMS@silicalite-1, (c,d) SG3@silicalite-1, and (e,f) SG20(II)@silicalite-1 after 2 and 4 successive secondary growth steps, respectively.

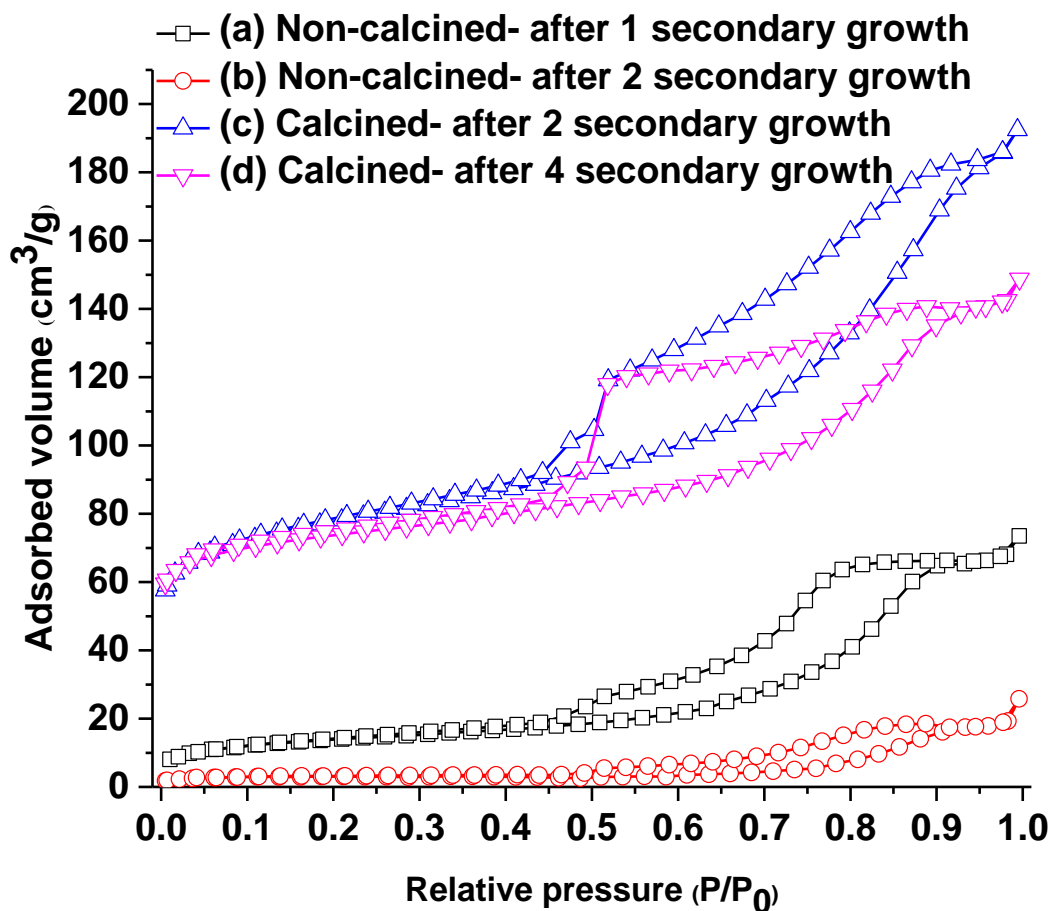
Masoumifard, N. *et al.*

Figure 2- Nitrogen adsorption/desorption isotherms measured at -196 °C for synthesized SG3@silicalite-1 (a,b) non-calcined samples after one and two successive secondary hydrothermal treatments, and (c,d) calcined samples after two and four successive secondary hydrothermal treatments.

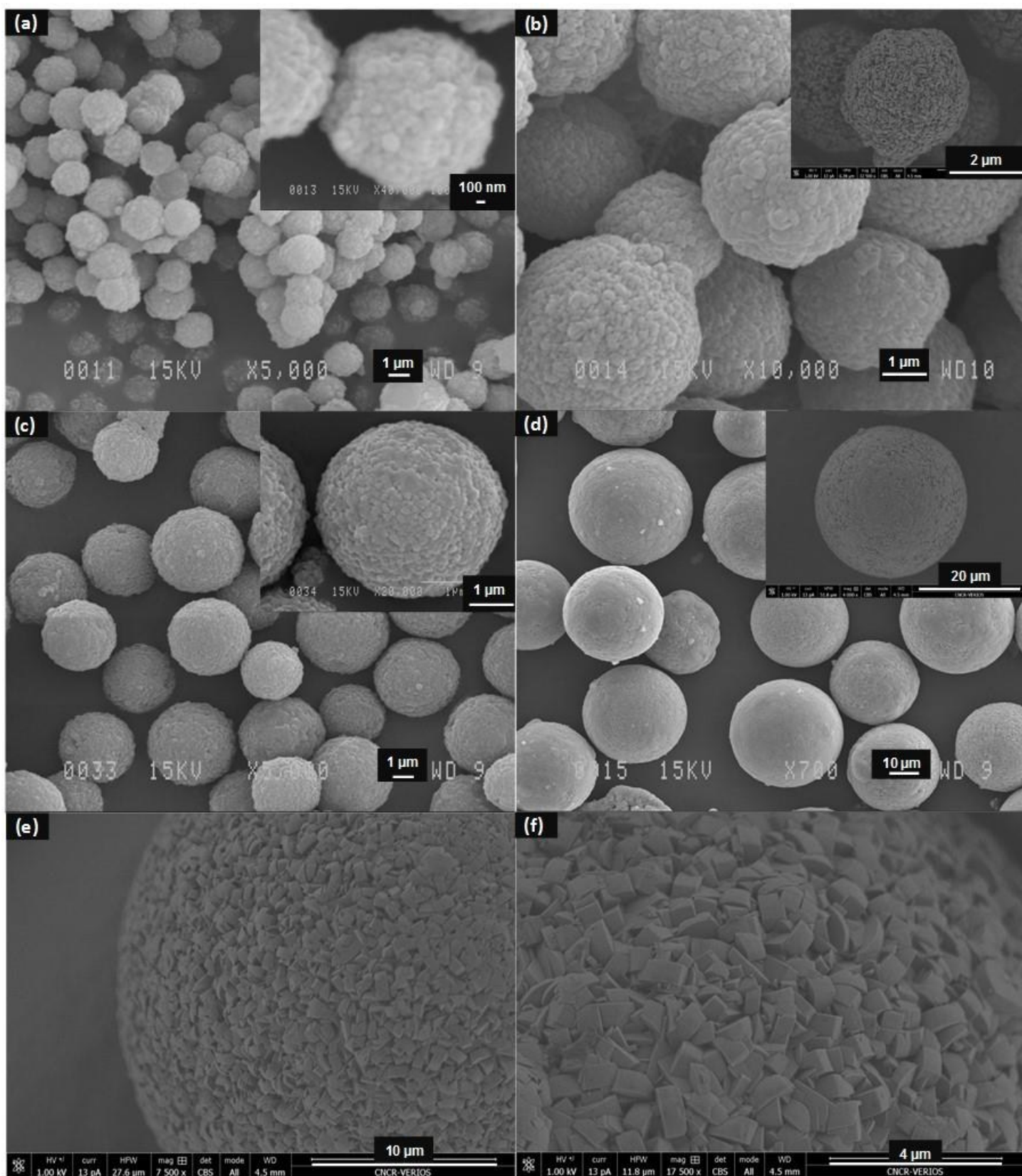
Masoumifard, N. *et al.*

Figure 3- SEM images of (a) Ti,HMS@silicalite-1, (b) Co,SG3@silicalite-1, (c) Mn,SG3@silicalite-1, (d-f) Co,SG20(I)@silicalite-1.

Masoumifard, N. *et al.*

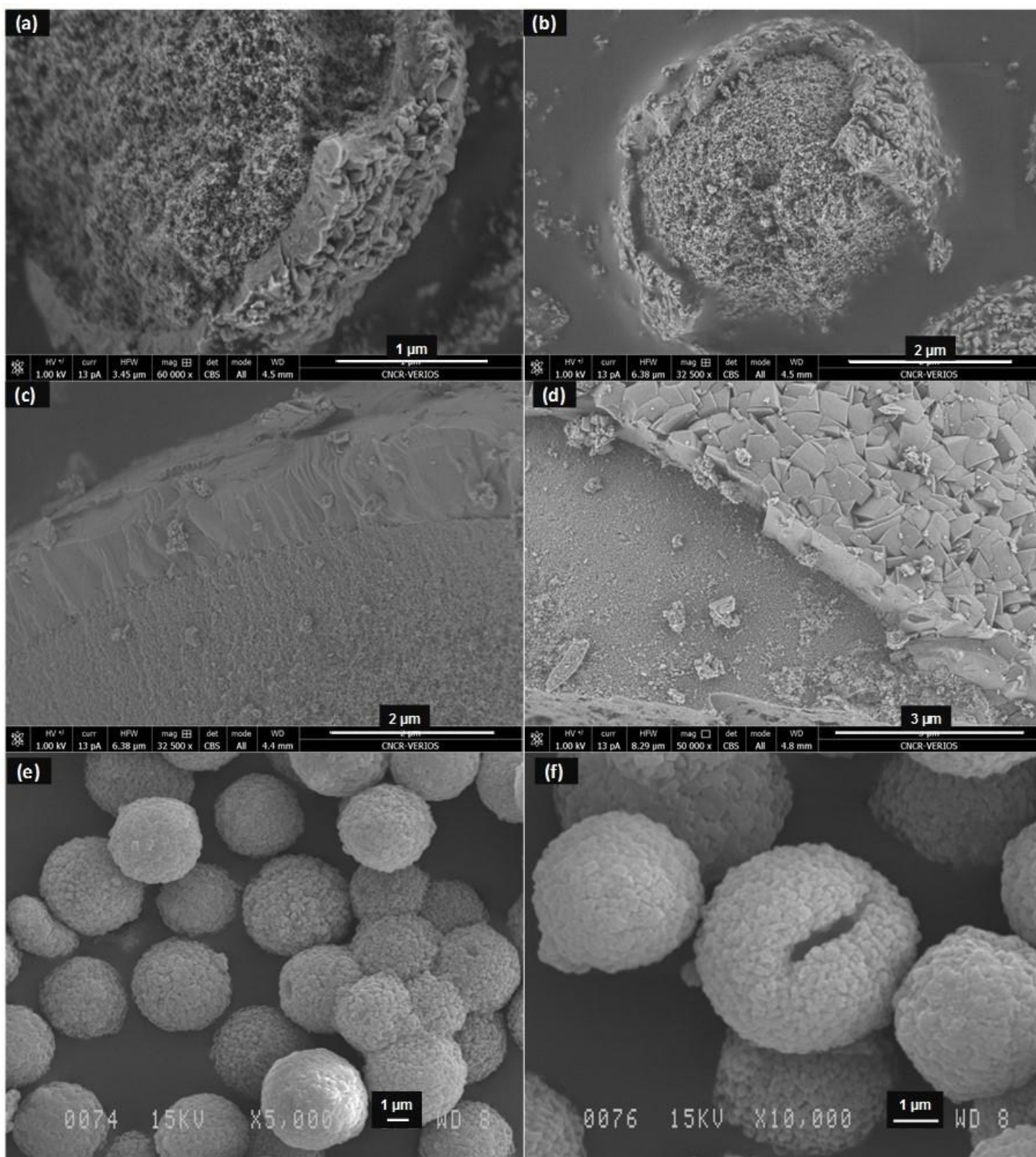


Figure 4- SEM images of (a,b) broken shell of Co,SG3@silicalite-1, (c,d) broken shell of Co,SG20@silicalite-1, and (e,f)Co,SG3@silicalite-1 after four secondary growth steps.

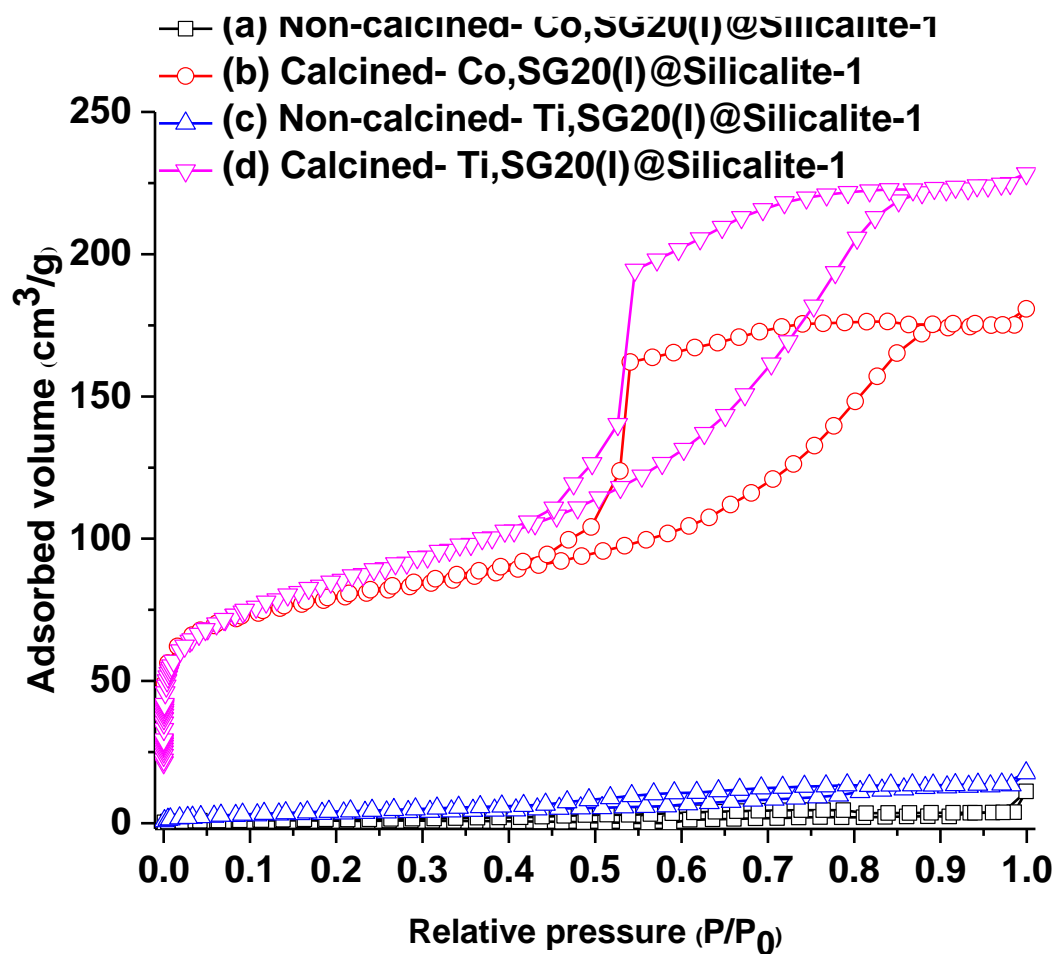


Figure 5- Nitrogen adsorption/desorption isotherms measured at  $-196\text{ }^\circ\text{C}$  for (a,b) Co,SG20(I)@silicalite-1 before and after calcination, and (c,d) Ti,SG20(I)@silicalite-1 before and after calcination.

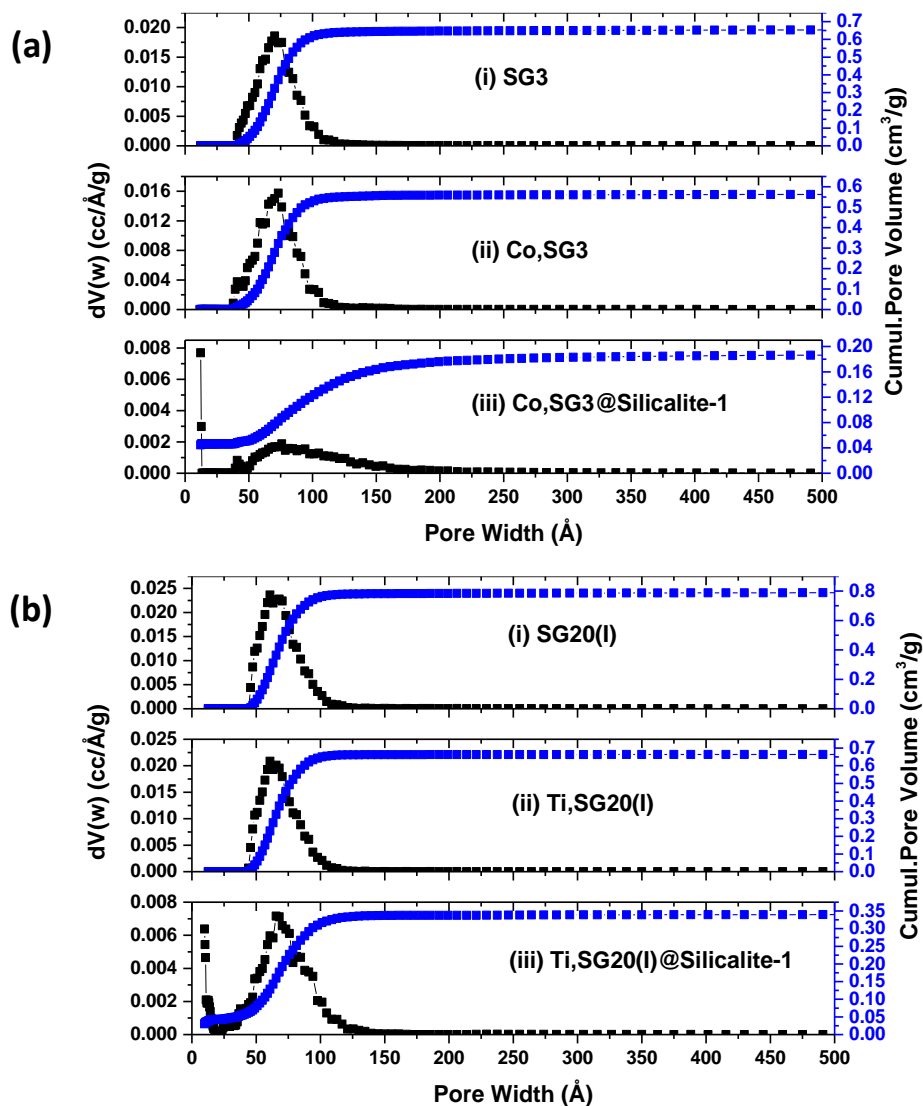
Masoumifard, N. *et al.*

Figure 6- NLDFT pore size distributions and cumulative pore volumes of (a) silica gel-3  $\mu\text{m}$  (SG3) (b) silica gel-20  $\mu\text{m}$  (SG20(l)), in pure form, after metal insertion and after shell formation, calculated from the adsorption branch of the isotherm by using the NLDFT method.

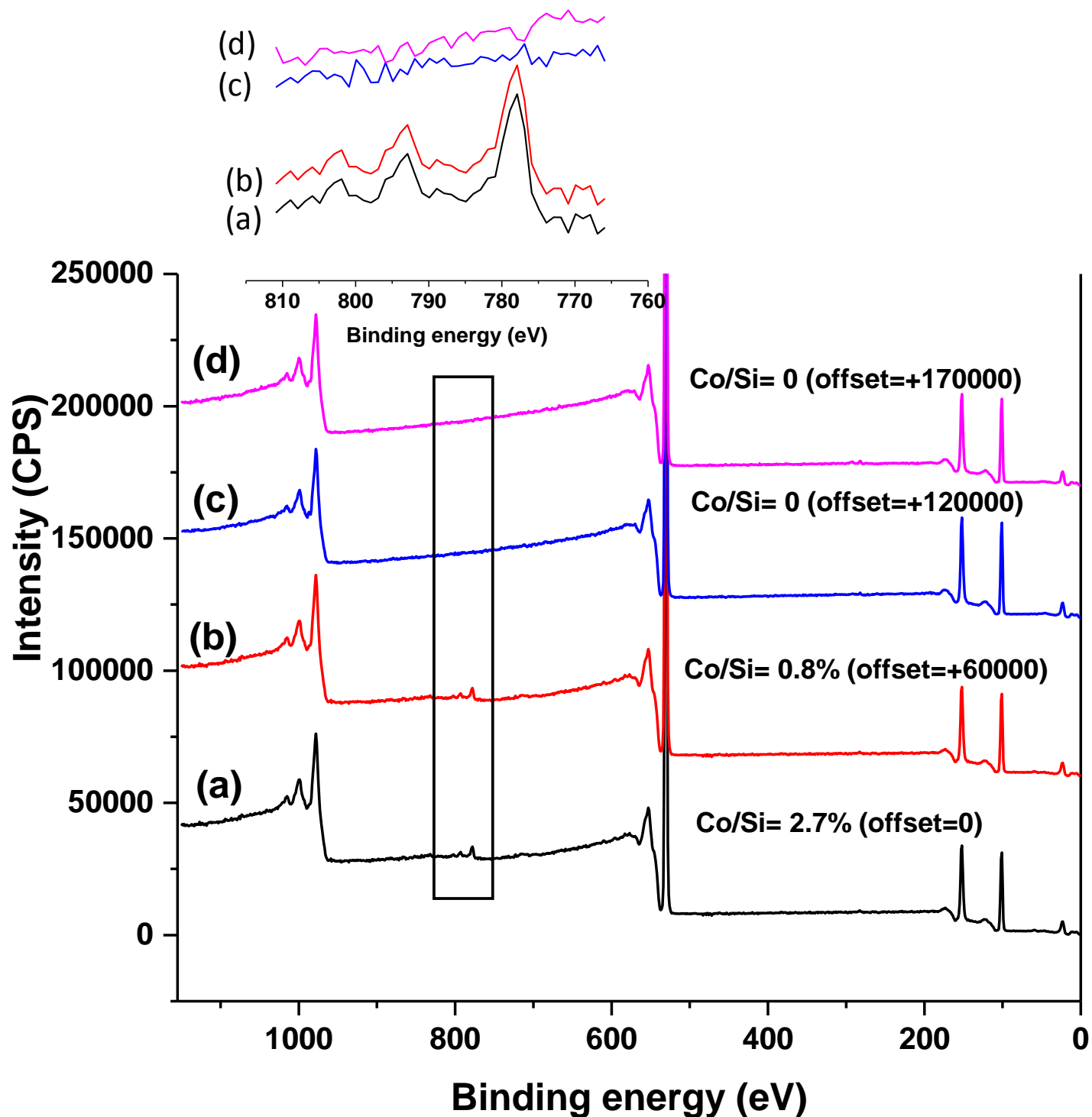


Figure 7- XPS survey spectra of (a) bare Co,SG20(I), (b) partially covered Co,SG3@silicalite-1, (c) fully covered Co,SG3@silicalite-1, and (d) fully covered Co,SG20(I)@silicalite-1 (survey scans were used for apparent concentrations, presented as Co/Si ratio in the graph).

Masoumifard, N. *et al.*

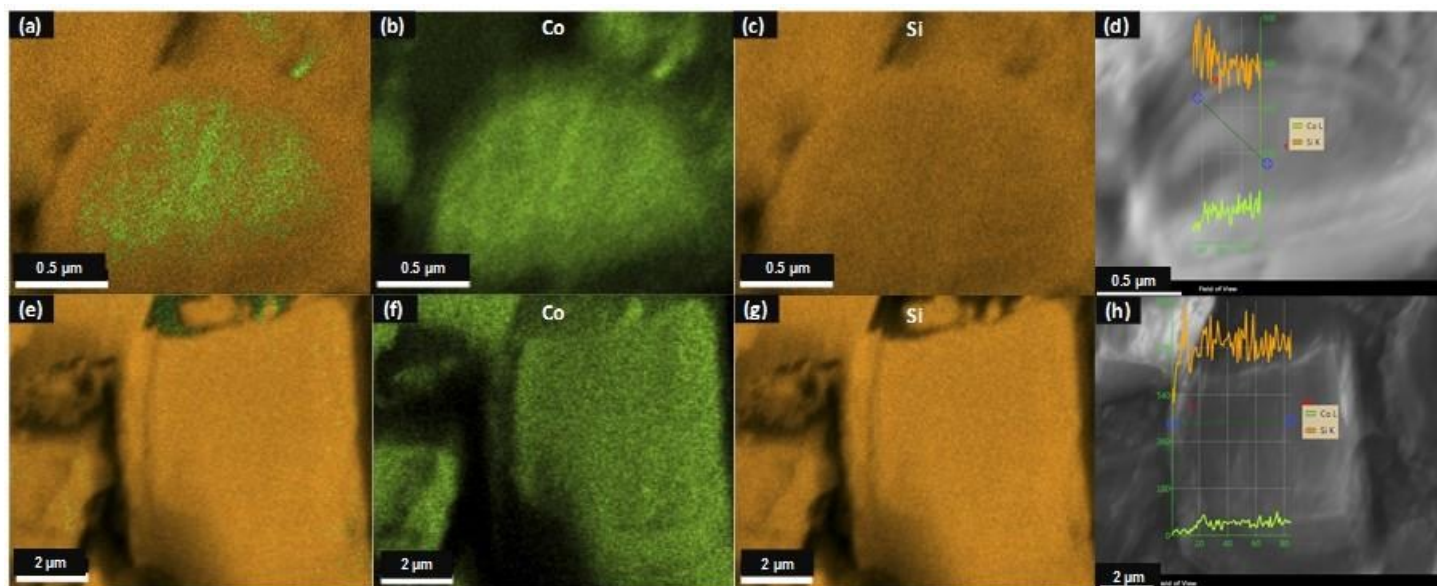
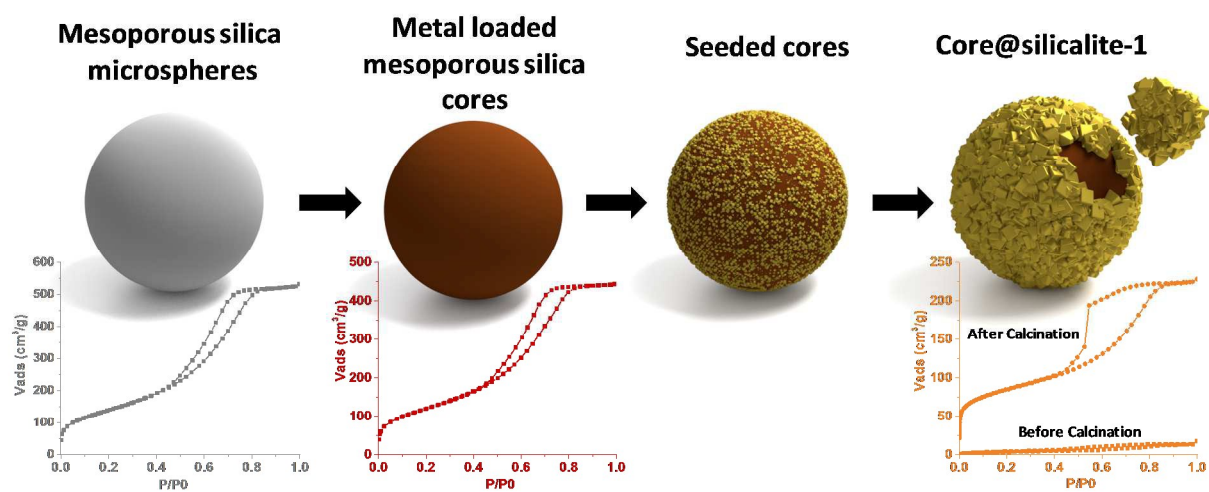


Figure 8- EDS elemental maps of (a-d) Co,SG3@silicalite-1 (Co/Si atomic ratio: 4%), and (e-h) Co,SG20(I)@silicalite-1 (Co/Si atomic ratio: 1%).

Masoumifard, N. *et al.***Table of content:****Graphical Abstract****Textual abstract**

Engineered silica@zeolite core-shell composites, possessing a hierarchical porosity in a shape selective manner, were synthesised by deposition of silicalite-1 nanocrystals over various mesoporous silica spheres, in either pure form or loaded with metal guest species.